RSC Advances

COMMUNICATION

View Article Online
View Journal | View Issue

Cite this: *RSC Adv.*, 2015, **5**, 86779

Received 31st August 2015
Accepted 7th October 2015

DOI: 10.1039/c5ra17661a

www.rsc.org/advances

Dual T_1/T_2 MRI contrast agent based on hybrid SPION@coordination polymer nanoparticles†

M. Borges,[a] S. Yu,[b] A. Laromaine,[b] A. Roig,[b] S. Suárez-García,[a] J. Lorenzo,[c] D. Ruiz-Molina[a] and F. Novio*[a]

We report a novel hybrid T_1/T_2 dual MRI contrast agent by the encapsulation of SPIONs (T_2 contrast agent) into an iron-based coordination polymer with T_1-weighted signal. This new hybrid material presents improved relaxometry and low cytotoxicity, which make it suitable for its use as contrast agent for MRI.

Magnetic resonance imaging (MRI) has become an important part of modern clinical imaging because of its non-invasive character, excellent spatial resolution, high soft tissue contrast and large penetration depth. Because one of the major limitations of MRI is its relative low sensitivity, the strategies of using complexes of paramagnetic Gd^{3+} or Mn^{2+} as T_1 contrast agents allow the enhancement of the signal causing a positive (or bright) MR image.[1] On the other hand, T_2 contrast agents that commonly consist of superparamagnetic nanoparticles (*e.g.*, iron-oxide) cause negative (or dark) MR images.[2] More recently, the increasing demand for sensitive MRI contrast agents has prompted attempts to combine T_1 and T_2 imaging in a synergistic manner to avoid possible MRI artifacts and to produce better images.[3] In recent years, different inorganic and inorganic–organic nanoprobes have been engineered to obtain a suitable contrast enhancement effect.[4]

Recently nanoscale coordination polymer particles (CPPs) have emerged as an alternative platform to provide new opportunities for engineering multifunctional systems. In general, CPPs exhibit high payloads of metal ion, high biocompatibility, low toxicity and offer the possibility to include additional functions.[5] Thus, the ability to incorporate diverse metals useful for MRI allows us to construct novel contrast agents for biomedical imaging. Hence, Gd^{3+} based coordination polymer nanoparticles have been described to improve contrast enhancement and decrease their toxicity.[6] However, even though Gd^{3+}-based CPPs may improve T_1 contrast efficiencies while minimizing toxic effects with respect to monomeric complexes, it is almost impossible to ensure the absence of free metal ions that induce toxic effects and systemic diseases.[7,8] Therefore, Mn^{2+}-based CPPs have been reported as an interesting alternative due to the lower toxicity of Mn^{2+} ions and their ability to provide efficient T_1-weighted contrast enhancement.[9] Still, though minimized, decomplexation *in vivo* of Mn^{2+} complexes generates free manganese ions that can also induce neurological degeneration or oxidative stress in cells.[10] Therefore, there is a real need for alternatives to these contrast agents such as the use of more biocompatible Fe^{3+} complexes.[11] However only few examples of MRI contrast agents based on iron coordination polymer particles are reported in spite of their relevance.[12,13] Moreover, as far as we know, none of such examples is based on a dual mode T_1/T_2 system, which is a real challenge nowadays in the cross-section of medicine and nanotechnology.[14]

Herein we report the use of catechol-based Fe^{3+} coordination polymer nanoparticles (**CPP-Fe**) as enhanced T_1-weighted MRI contrast agents. We show how these novel Fe^{3+} nanoparticles can be used as functional matrices to encapsulate superparamagnetic iron-oxide nanoparticles (SPIONs) during the polymerization precipitation process (Fig. 1).[15] The combination of SPIONs as powerful T_2-negative contrasts agent[16] with the excellent T_1-positive contrast responses of the **CPP-Fe** nanoparticles results in the formation of a novel hybrid material with optimal dual T_1/T_2 responses.

In a typical experiment for the synthesis of **CPP-Fe** nanoparticles, an aqueous solution of $Fe(CH_3COO)_2 \cdot xH_2O$ was added to an ethanolic solution combining two co-ligands, *i.e.* 3,4-dihydroxycinnamic acid (dhc) and 1,4-bis(imidazol-1-ylmethyl)benzene (bix), used as a counter ligand to induce

[a]*ICN2-CSIC – Catalan Institute of Nanoscience and Nanotechnology (ICN2), CSIC and The Barcelona Institute of Science and Technology, Campus UAB, Bellaterra, Barcelona 08193, Spain. E-mail: fnovio@cin2.es*

[b]*ICMAB-CSIC – Institut de Ciència de Materials de Barcelona, Consejo Superior de Investigaciones Científicas, Campus de la UAB, 08193 Bellaterra, Barcelona, Spain*

[c]*IBB-UAB – Institut de Biotecnologia i de Biomedicina. Departament de Bioquímica i Biologia Molecular. Universitat Autònoma de Barcelona, 08193 Bellaterra, Barcelona, Spain*

† Electronic supplementary information (ESI) available: Synthetic and experimental procedures, SEM and TEM images, FT-IR, UV-Vis, Mössbauer and EDX spectra. See DOI: 10.1039/c5ra17661a

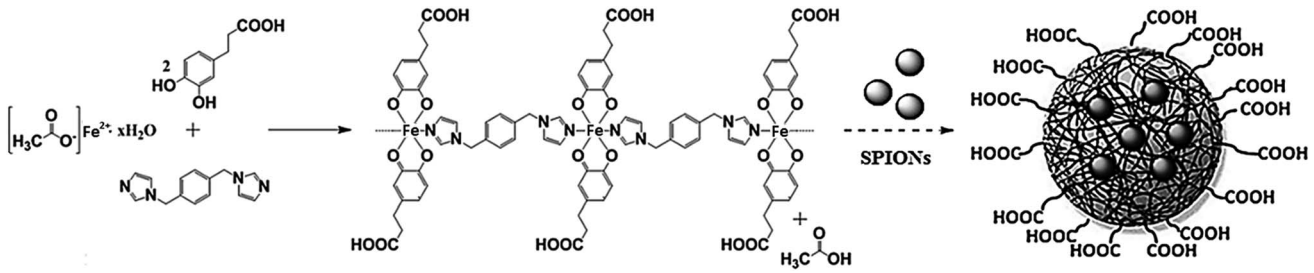

Fig. 1 Synthesis of **CPP-Fe** and *in situ* encapsulation of SPIONS to generate the hybrid nanomaterial **SPION@CPP-Fe**.

polymerization.[17,18] Although the original source of iron is an Fe^{2+} salt, the complex was stabilized as high-spin Fe^{3+} as shown by Mössbauer spectroscopy (see ESI, Fig. S1†). This electronic modification results from a redox interplay between the metal ion and the electroactive catechol ligands in air as previously reported.[19] SPION nanoparticles with a narrow size distribution (6.0 ± 1.0 nm, as determined from TEM), and good dispersion in water (for complete characterization see ESI, Fig. S2†), were synthesized applying a microwave-assisted thermal decomposition route.[20] Afterwards, the encapsulation of SPIONs within **CPP-Fe** nanoparticles was carried out. In a typical experiment, 5 mL of SPIONs dispersed in water (0.3 mM, see ESI, Fig. S3†) and iron acetate (0.125 mmol, 1 mL H_2O) were mixed in an ultrasound bath (separate addition of aqueous solutions of SPIONs and iron salt resulted in low encapsulation rates, increase of particle aggregation and a broad size distribution). After a couple of minutes, the mixture was added to 7.5 mL of ethanol containing the bix ligand (0.125 mmol) and 45 mg of dhc (0.25 mmol). The reaction solution turned dark blue and led to rapid formation of a precipitate that was kept for 30 minutes under ultrasonic mixing (magnetic stirring was discarded upon yielding worse size dispersions and lower encapsulation yields). The solid product was centrifuged and washed with water and ethanol 3 times to eliminate the unreacted reagents. Finally, the solvent was removed and the solid was dried under vacuum. The resulting hybrid material **SPION@CPP-Fe** consists of nanoparticles with an average size of 64 ± 8 nm as estimated from STEM images (Fig. 2) and 86 ± 12 nm from DLS measurements in water (for full characterization see ESI, Fig. S4†). XRD measurements revealed that the characteristic diffraction pattern of the SPIONs is retained after encapsulation (the **CPP-Fe** are amorphous). Energy dispersive X-ray (EDX) microanalysis shows the presence of iron, oxygen, nitrogen, and carbon. The amount of SPIONs present in the hybrid nanoparticles was quantitatively determined by thermogravimetric analysis (TGA) carried out under an air flow and by ICP-MS. The TGA analysis after complete combustion of the samples (900 °C) indicates a difference in remaining weight between **CPP-Fe** and **SPION@CPP-Fe** of 7.2%. Considering the chemical composition of SPIONs (Fe_2O_3), the percentage of iron from encapsulated SPIONs is 4.1%. This result is in agreement with the ICP-MS data that indicate an iron percentage of 3.8% ascribed to SPIONs when comparing **CPP-Fe** with **SPION@CPP-Fe.**

Stable colloidal suspensions of the **SPION@CPP-Fe** nanoparticles are obtained at concentrations below 20 mM (Fig. 2d) while higher concentrations lead to an aggregation and precipitation process. The stability of the particles can be modulated upon pH variations. Indeed, protonation or deprotonation of the surface carboxylic groups at different pHs enable control over the colloidal dispersion in water mainly by electrostatic repulsions.[17] For this, nanoparticles were dispersed in different PBS buffers (pH: 5.0, 7.3, 9.0). The corresponding Z-potential *vs.* pH are presented in Fig. 2e (a comparison between DLS and Z-potential measurements is reported in ESI, Fig. S5†). A pH increase from 7.3 to 9.0 leads to more negative zeta-potential values, from −30 ± 6 mV to −40 ± 4 mV respectively, and consequently to a decrease of particle aggregation. On the contrary, a pH decrease from 7.3 to 5.0 induces

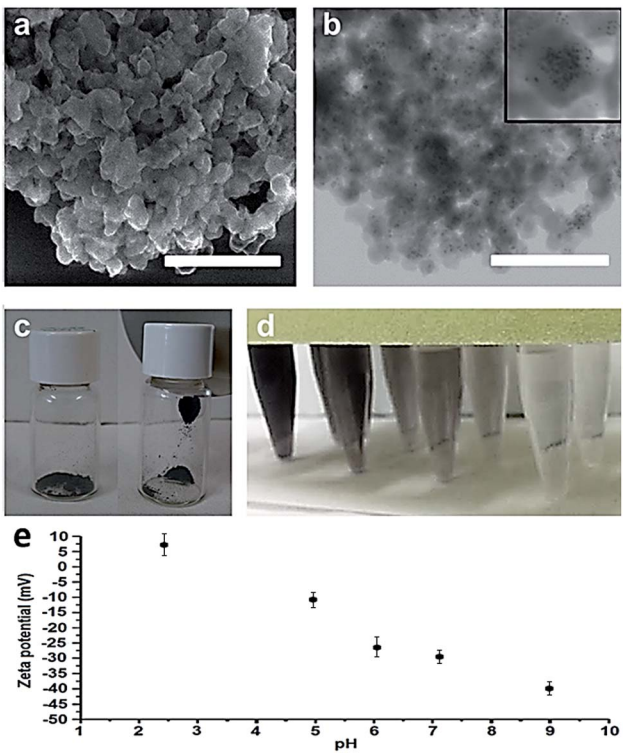

Fig. 2 STEM images in: (a) scanning mode, (b) bright-field transmission mode (inset: zoom of discrete hybrid NPs). Scale bar = 1 μm; (c) image of solid **SPION@CPP-Fe** nanoparticles attracted by a magnet; (d) aqueous dispersions of different concentrations (1, 5, 10, and 25 mM from right to left) of **CPP-Fe** (rear) and **SPION@CPP-Fe** (front); (e) Z-potential measurements for **SPION@CPP-Fe** as function of pH.

protonation of the surface carboxylate groups, leading to a zeta-potential value close to zero with consequent aggregation and precipitation. This pH-induced process is fully reversible in the pH range 4–9; beyond this range, decomposition of the nanoparticles is detected by STEM and FT-IR. In the same way, STEM analyses corroborate the permanence of SPIONs inside the polymer matrix in the pH range 6–9 for several days.

Finally, the longitudinal r_1 and transverse r_2 relaxation rates for different concentrations of **CPP-Fe** and **SPION@CPP-Fe** were measured in solution under an external magnetic field of 7 Teslas in two phantom sequences (Fig. 3). The nanoprobes were dispersed in a pH = 9 PBS buffer to ensure a good colloidal stability. The obtained relaxation rate values were plotted *versus* the total concentrations of iron and the relative iron concentration reporting good linear correlations (see ESI, Fig. S6†). Since for both contrast agents (**CPP-Fe** and SPIONs), iron is the active metal, the relaxivity values will take into account the relative iron concentration (*i.e.* r_1 is related to iron concentration in **CPP-Fe** and r_2 is related to iron concentration from encapsulated SPIONs). Relaxivity values referred to the total concentration of iron in the hybrid nanoparticles are also presented in ESI, Fig. S6.†

Notably, **CPP-Fe** nanoparticles exhibit a signal enhancement in a concentration-dependent manner and a good T_1 positive contrast (r_1 = 4.4 mM^{-1} s^{-1}). This value is comparable to commonly used gadolinium contrast agents[21,22] and in the same range of the commercial compound Gd-DTPA[20] (3.3 mM^{-1} s^{-1} at pH = 7; 4.3 mM^{-1} s^{-1} at pH = 9, measured in the present work), which make these nanoparticles an alternative contrast agent to Gd-based compounds. As the relaxivity measurements in buffer solution for **CPP-Fe** at pH = 7 presented some problems of reproducibility because the limit stability of the colloidal solution, the corresponding relaxation measurements at physiological pH = 7.2 were performed in agarose gel (r_1 = 5.9 mM^{-1} s^{-1}) and compared with the commercial gadolinium compound Magnevist® in identical conditions (r_1 = 4.3 mM^{-1} s^{-1}). As showed, this value represents an increased signal intensity in comparison with the commercial probes. Moreover, r_1 value of **CPP-Fe** is comparable or even higher than those found for previously reported iron-based coordination polymers,[12,13] or molecular complexes,[23] which exhibit r_1 values up to 3 mM^{-1} s^{-1}. Such excellent response, although the Fe^{3+} metal ions are expected to have a completed coordination sphere, can be attributed to the use of catechol-based ligands, which have already been reported to maximize second-sphere interactions with water molecules, and therefore to enhance T_1, through hydrogen bonding with the oxygen atoms of the Fe–O–R linkages.[24]

The r_1 relaxivity value for the hybrid material **SPION@CPP-Fe** is 2.8 mM^{-1} s^{-1} (2.1 mM^{-1} s^{-1} based on the total concentration of Fe), which is lower than that obtained for the **CPP-Fe** nanoparticles. Such reduction in longitudinal relaxivity can be due to the local magnetic field generated by the SPION nanoparticles that slightly perturbs the relaxation process of the paramagnetic T_1 contrast material, and therefore induces its quenching.[25] On the other hand, the r_2 relaxivity value of **SPION@CPP-Fe** is 185.3 mM^{-1} s^{-1}, which as expected is considerably higher than the r_2 transversal relaxivity of the **CPP-Fe** nanoparticles (10.9 mM^{-1} s^{-1}) thanks to the encapsulated SPIONs. Moreover, such value is comparable to that obtained for the commercial agent RESOVIST® (183.4 mM^{-1} s^{-1}) and even higher than that reported for non-encapsulated SPION nanoparticles (140 mM^{-1} s^{-1}).[26] This variation in magnetic relaxivity could be related to confinement of a given number of SPIONs in each CPP nanoparticle, and thus their enhanced ability to decrease the transverse relaxation time of protons in surrounding water.[27] These results also confirm that the paramagnetic **CPP-Fe** polymer does not interfere with the T_2 relaxation processes of the SPIONs. Indeed, the high transverse relaxation (r_2) and transverse to longitudinal relaxation ratio (r_2/r_1 = 66.2, related to relative iron concentration; r_2/r_1 = 23.5 related to the total iron concentration) exhibited by the **SPION@CPP-Fe** nanoparticles indicate its potential use as T_2 contrast agents.[28]

To compare the effect on cell viability of the **CPP-Fe** nanosystems with a commercial Gd-compound contrast agent (Magnevist®), the cytotoxicity against HeLa cells was studied at incubation times of 24 and 72 h. The concentrations were referenced to the metal content. For the determination of the toxicity effect on the cell line, the PrestoBlue reagent assay based on the metabolic reduction of resazurin on resorufin was used. HeLa cells were treated over 24 h with increasing doses of the **CPP-Fe** nanoparticles or Magnevist®. Each sample was tested in quadruplicate. The results indicate that HeLa cells retained more than 90% viability for both systems, in comparison with untreated cells, at concentrations below 75 μM after 24 h of

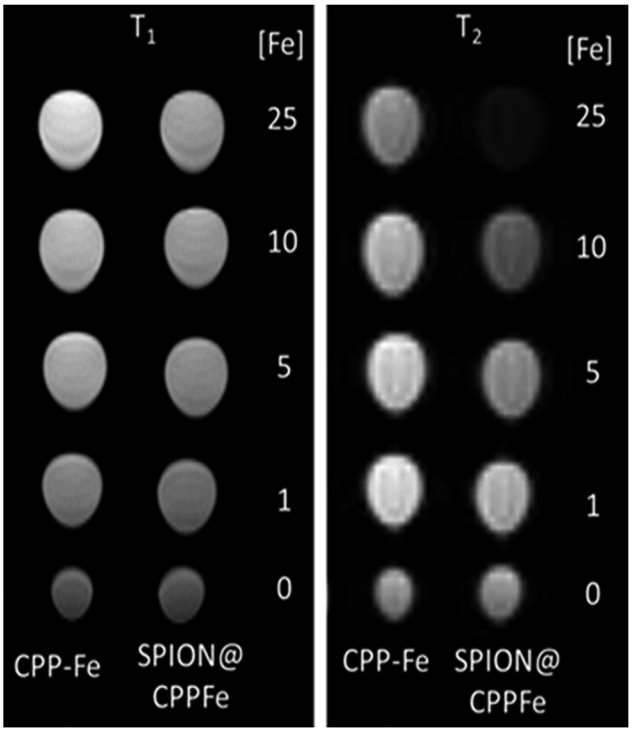

Fig. 3 ^{1}H MRI T_1 and T_2 phantoms maps of **CPP-Fe** and **SPION@CPP-Fe** nanoparticles in a pH = 9 PBS buffer at different concentrations (mM).

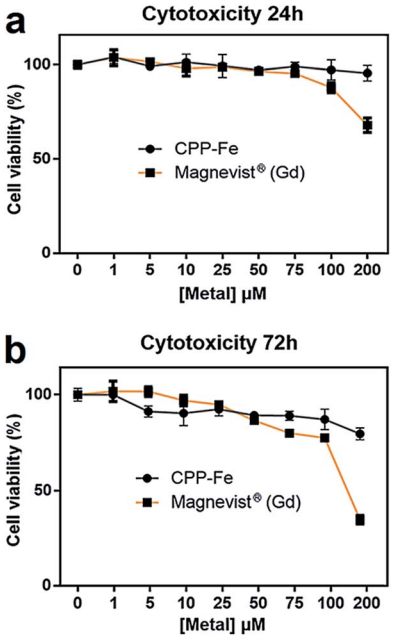

Fig. 4 Cytotoxicity of CPP-Fe and commercial gadolinium contrast agent (Magnevist®) in HeLa cells measured by the resazurin PrestoBlue assay. CPP-Fe and Magnevist were added in concentrations ranking from 1 to 200 μM and then incubated for (a) 24 h or (b) 72 h after incubation for (a) 24 h and (b) 72 h.

incubation (Fig. 4a). However, when the metal concentration was increased above 100 μM, notable differences in cytotoxicity were observed, namely **CPP-Fe** maintained low cytotoxicity levels whereas the gadolinium compound started to show severe cytotoxic effect. After 72 h of incubation (Fig. 4b), the results shows again low toxic effect for **CPP-Fe**, close to 85% of cell viability at 200 μM. On the contrary, the commercial gadolinium compound presents a cell viability of less than 30% for the highest concentration used in this study. It could be suggested that the stability of the **CPP-Fe** nanoparticles and the chemical composition result in low toxicity. Complementarily, cytotoxicity studies with **SPION@CPP-Fe** nanoparticles showed identical dose-dependent cell viability to that obtained for **CPP-Fe**.

Conclusions

Fe^{3+} coordination polymer nanoparticles (**CPP-Fe**) have been developed as excellent T_1 contrast probes with responses comparable to those of commercial gadolinium compounds or related Fe^{3+} complexes. The safety of MRI contrast agents is an important parameter for clinical applications, which has not yet been solved with current Gd-based compounds. Indeed, toxic Gd(III) ions may be released from some of the chelates by transmetallation with other metal ions such as Zn^{2+}, Ca^{2+} and Cu^{2+} in the body. Furthermore, protonation of the ligands at low pH may cause chelate dissociation,[29] which may induce serious adverse reactions such as nephrogenic systemic fibrosis.[30] In the present study, we have developed nanosystems with notable robustness in a wide range of pH and containing Fe(III) nontoxic metal ions.

Moreover, taking advantage of the chemical flexibility of this new family of MRI probes we have obtained hybrid nanoparticles with dual T_1/T_2 responses by encapsulation of SPIONs. Even though the value of longitudinal relaxivity (r_1) is smaller for the hybrid nanoparticles than for **CPP-Fe**, the **SPION@CPP-Fe** nanoparticles present suitable r_1 and r_2 values to be used as efficient dual T_1/T_2 contrast agents.

Acknowledgements

This work was supported by project MAT2012-38318-C03-02 and MAT2012-35324 and BIO2013-44973-R from the Spanish Government and FEDER funds. F.N. thanks the Ministerio de Ciencia e Innovación (MICINN) for a postdoctoral JdC fellowship and A.L. thanks Ramon y Cajal grant RYC-2010-06082. SM.Y. acknowledges the China Scholarship Council fellowship (201206150053). Authors also thank MP1202 and TD1004 Cost Actions. ICN2 acknowledges support from the Severo Ochoa Program (MINECO, Grant SEV-2013-0295). MR studies were carried out at the joint NMR facility of UAB and CIBER-BBN, Unit 25 of NANBIOSIS, with a 7T horizontal.

Notes and references

1 E. J. Rummeny, P. Reimer and W. Heindel, in *MR Imaging of the Body*, Thieme Medical Publishers, New York, 1st edn, 2009, p. 690.
2 S. Laurent, D. Forge, M. Port, A. Roch, C. Robic, L. Vander Elst and R. N. Muller, *Chem. Rev.*, 2008, **108**, 2064–2110.
3 T.-H. Shin, J.-S. Choi, S. Yun, I.-S. Kim, H.-T. Song, Y. Kim, K. I. Park and J. Cheon, *ACS Nano*, 2014, **8**, 3393–3401.
4 E. Peng, F. Wang and J. M. Xue, *J. Mater. Chem. B*, 2015, **3**, 2241–2276.
5 (*a*) F. Novio, J. Simmchen, N. Vázquez-Mera, L. Amorín-Ferré and D. Ruiz-Molina, *Coord. Chem. Rev.*, 2013, **257**, 2839–2847; (*b*) J. D. Rocca, D. Liu and W. Lin, *Acc. Chem. Res.*, 2011, **44**, 957–968.
6 (*a*) S. Okada, S. Mizukami and K. Kikuchi, *Bioorg. Med. Chem.*, 2012, 769–774; (*b*) M. D. Rowe, D. H. Thamm, S. L. Kraft and S. G. Boyes, *Biomacromolecules*, 2009, **10**, 983–993; (*c*) M. D. Rowe, Ch.-Ch. Chang, D. H. Thamm, S. L. Kraft, J. F. Harmon, A. P. Vogt, B. S. Sumerlin and S. G. Boyes, *Langmuir*, 2009, **25**, 9487–9499; (*d*) Y. Guari, J. Larionova, M. Corti, A. Lascialfari, M. Marionone, G. Poletti, K. Mlvinger and Ch. Gérin, *Dalton Trans.*, 2008, 3658–3660; (*e*) K. M. L. Taylor, A. Jin and W. Lin, *J. Am. Chem. Soc.*, 2008, **47**, 7722–7725.
7 (*a*) Z. P. Xu, N. D. Kurniawan, P. F. Bartlett and G. Q. Lu, *Chem.–Eur. J.*, 2007, **13**, 2824–2830; (*b*) W. P. Cacheris, S. C. Quay and S. M. Rocklage, *Magn. Reson. Imaging*, 1990, **8**, 467–481.
8 (*a*) M. A. Sieber, T. Steger-Hartmann, P. Lengsfeld and H. Pietsch, *J. Magn. Reson. Imag.*, 2009, **30**, 1268–1276; (*b*) M. R. Prince, H. L. Zhang, J. C. Prowda, M. E. Grossman and D. N. Silvers, *Radiographics*, 2009, **29**, 1565–1574; (*c*) J. M. Idee, M. Port, A. Dencausse, E. Lancelot and C. Corot, *Radiol. Clin.*, 2009, **47**, 855–869.

9 (*a*) D. Liu, Ch. He, Ch. Poon and W. Lin, *J. Mater. Chem.*, 2014, **2**, 8249–8255; (*b*) K. M. L. Taylor, W. J. Rieter and W. Lin, *J. Am. Chem. Soc.*, 2008, **130**, 14358–14359.

10 (*a*) A. S. Hazell, *Neurochem. Int.*, 2002, **41**, 271–277; (*b*) K. Eriksson, A. W. Dobson, D. C. Dorman and M. Aschner, *Sci. Total Environ.*, 2004, **409**, 334–335.

11 (*a*) J. A. Davies, S. G. Dutremez, C. M. Hockensmith, R. Keck, N. Richardson, S. Selman, D. A. Smith, C. W. Ulmer II, L. S. Wheatley and J. Zeiss, *Acad. Radiol.*, 1996, **3**, 936–945; (*b*) M. Botta, *Eur. J. Inorg. Chem.*, 2000, 399–407; (*c*) S. Aime, M. Botta, E. Terreno, P. L. Anelli and F. Uggeri, *Magn. Reson. Med.*, 1993, **30**, 583–591; (*d*) P. Caravan, M. T. Greenfield, X. Li and A. D. Sherry, *Inorg. Chem.*, 2001, **40**, 6580–6587; (*e*) J.-X. Yu, V. D. Kodibagkar, L. Liu, Z. Zhang, L. Liu, J. Magnusson and Y. Liu, *Chem. Sci.*, 2013, **4**, 2132–2142; (*f*) J.-X. Yu, P. K. Gulaka, L. Liu, V. D. Kodibagkar and R. P. Mason, *ChemPlusChem*, 2012, **77**, 370–378; (*g*) D. D. Schwert, J. A. Davies and N. Richardson, *Top. Curr. Chem.*, 2002, **221**, 165–199.

12 J. Guo, Y. Ping, H. Ejima, K. Alt, M. Meissner, J. J. Richardson, Y. Yan, K. Peter, D. von Elverfeldt, C. E. Hagemeyer and F. Caruso, *Angew. Chem., Int. Ed.*, 2014, **53**, 5546–5551.

13 J. Wang, A. de Keizer, H. P. van Leeuwen, Y. Yan, F. Vergeldt, H. van As, P. H. H. Bomans, N. A. J. M. Sommerdijk, M. A. C. Stuart and J. van der Gucht, *Langmuir*, 2011, **27**, 14776–14782.

14 (*a*) H. Yang, Ch. Qin, Ch. Yu, Y. Lu, H. Zhang, F. Xue, D. Wu, Z. Zhou and Sh. Yang, *Adv. Funct. Mater.*, 2014, **24**, 1738–1747; (*b*) Z. Wang, J. Liu, T. Li, J. Liu and B. Wang, *J. Mater. Chem. B*, 2014, **2**, 4748–4753; (*c*) A. Szpak, S. Fiejdasz, W. Prendota, T. Straczek, C. Kapusta, J. Szmyd, M. Nowakowska and S. Zapotoczny, *J. Nanopart. Res.*, 2014, **16**, 2678; (*d*) K. H. Bae, Y. B. Kim, Y. Lee, J. Y. Hwang, H. Park and T. G. Park, *Bioconjugate Chem.*, 2010, **21**, 505–512; (*e*) J. T.-W. Wang, *et al.*, *Adv. Funct. Mater.*, 2014, **24**, 1880–1894.

15 (*a*) M. Saikia, D. Bhuyan and L. Saikia, *New J. Chem.*, 2015, **39**, 64–67; (*b*) S. Xu, J. Liu, D. Li, L. Wang, J. Guo, Ch. Wang and Ch. Chen, *Biomaterials*, 2014, **35**, 1676–1685; (*c*) Y. Kim, Y. S. Choi, H. J. Lee, H. Yoon, Y. K. Kim and M. Oh, *Chem. Commun.*, 2014, **50**, 7617–7620; (*d*) C. M. Doherty, D. Buso, A. J. Hill, S. Furukawa, S. Kitagawa and P. Falcaro, *Acc. Chem. Res.*, 2014, **47**, 396–405; (*e*) Y. Liu and Z. Tang, *Adv. Mater.*, 2013, **25**, 5819–5825; (*f*) F. Ke, L. –G. Qiu, Y. –P. Yuan, X. Jiang and J. –F. Zhu, *J. Mater. Chem.*, 2012, **22**, 9497–9500; (*g*) Sh. Xu, L. You, P. Zhang, Y. Zhang, J. Guo and Ch. Wang, *Chem. Commun.*, 2013, **49**, 2427–2429; (*h*) S. B. Kim, Ch. Cai, Sh. Sun and D. A. Sweigart, *Angew. Chem., Int. Ed.*, 2009, **48**, 2907–2910.

16 (*a*) E. Taboada, E. Rodríguez, A. Roig, J. Oro, A. Roch and R. N. Muller, *Langmuir*, 2007, **23**, 4583–4588; (*b*) Z. R. Stephen, F. M. Kievit and M. Zhang, *Mater. Today*, 2011, **14**, 330–338; (*c*) O. Veiseh, J. W. Gunn and M. Zhang, *Adv. Drug Delivery Rev.*, 2010, **62**, 284–304; (*d*) E. Terreno, D. D. Castelli, A. Viale and S. Aime, *Chem. Rev.*, 2010, **110**, 3019–3042; (*e*) S. Laurent, D. Forge, M. Port, A. Roch, C. Robic, C. L. Vander Elst and R. N. Muller, *Chem. Rev.*, 2008, **108**, 2064–2110; (*f*) T. D. Schladt, K. Schneider, H. Schild and W. Tremel, *Dalton Trans.*, 2011, **40**, 6315–6343.

17 F. Novio, J. Lorenzo, F. Nador, K. Wnuk and D. Ruiz-Molina, *Chem.–Eur. J.*, 2014, **20**, 15443–15450.

18 F. Novio and D. Ruiz-Molina, *RSC Adv.*, 2014, **4**, 15293–15296.

19 D. H. Jo, Y.-M. Chiou and L. Que Jr, *Inorg. Chem.*, 2001, **40**, 3181–3190.

20 (*a*) O. Pascu, E. Carenza, M. Gich, S. Estradé, F. Peiró, G. Herranz and A. Roig, *J. Phys. Chem. C*, 2012, **116**, 15108–15116; (*b*) S. Yu, A. Laromaine and A. Roig, *J. Nanopart. Res.*, 2014, **16**, 2484; (*c*) L. Gonzalez-Moragas, S.-M. Yu, N. Murillo-Cremaes, A. Laromaine and A. Roig, *Chem. Eng. J.*, 2015, **281**, 87–95.

21 P.-C. Chu, W.-Y. Chai, H.-Y. Hsieh, J.-J. Wang, S.-P. Wey, C.-Y. Huang, K.-C. Wei and H.-L. Liu, *BioMed Res. Int.*, 2013, 627496.

22 C. F. G. C. Geraldes and S. Laurent, *Contrast Media Mol. Imaging*, 2009, **4**, 1–23.

23 (*a*) N. Richardson, J. A. Daviesa and B. Radüchel, *Polyhedron*, 1999, **18**, 2457–2482; (*b*) E. Rodríguez, R. V. Simoes, A. Roig, E. Molins, N. Nedelko, A. Slawska-Waniewska, S. Aime, C. Arús, M. E. Cabañas, C. Sanfeliu, S. Cerdán and M. L. García-Martín, *Magn. Reson. Mater. Phys., Biol. Med.*, 2007, **20**, 27–37.

24 D. D. Schwert, N. Richardson, G. Ji, B. Radüchel, W. Ebert, P. E. Heffner, R. Keck and J. A. Davies, *J. Med. Chem.*, 2005, **48**, 7482–7485.

25 J. S. Choi, J. H. Lee, T. H. Shin, H. T. Song, E. Y. Kim and J. Cheon, *J. Am. Chem. Soc.*, 2010, **132**, 11015–11017.

26 E. Carenza, V. Barceló, A. Morancho, J. Montaner, A. Rosell and A. Roig, *Acta Biomater.*, 2014, **10**, 3775–3785.

27 (*a*) M. K. Nkansah, D. Thakral and E. M. Shapiro, *Magn. Reson. Med.*, 2011, **65**, 1776–1785; (*b*) E. Taboada, R. Solanas, E. Rodríguez, R. Weissleder and A. Roig, *Adv. Funct. Mater.*, 2009, **19**, 2319–2324; (*c*) F. Y. Cheng, S. P. Wang, C. H. Su, T. L. Tsai, P. C. Wu, D. B. Shieh, J. H. Chen, P. C. Hsieh and C. S. Yeh, *Biomaterials*, 2008, **29**, 2104–2112; (*d*) C. Xu, D. Miranda-Nieves, J. A. Ankrum, M. E. Matthiesen, J. A. Phillips, I. Roes, G. R. Wojtkiewicz, V. Juneja, J. R. Kultima, W. Zhao, P. K. Vemula, C. P. Lin, M. Nahrendorf and J. M. Karp, *Nano Lett.*, 2012, **12**, 4131–4139.

28 S. Srivastava, R. Awasthi, D. Tripathi, M. K. Rai, V. Agarwal, V. Agrawal, N. S. Gajbhiye and R. K. Gupta, *Small*, 2012, **8**, 1099–1109.

29 (*a*) S. Laurent, L. V. Elst, F. Copoix and R. N. Muller, *Invest. Radiol.*, 2001, **36**, 115–122; (*b*) S. A. Greenberg, *Radiology*, 2010, **257**, 670–673.

30 H. S. Thomsen, *Eur. J. Radiol.*, 2006, **16**, 2619–2621.